

## Evaluation of cyclic fracture in perforated beams using micromechanical fatigue model

Saeed Erfani\* and Vahid Akrami<sup>a</sup>

Civil Engineering Department, Amirkabir University of Technology, Tehran, Iran

(Received September 02, 2015, Revised December 23, 2015, Accepted December 29, 2015)

**Abstract.** It is common practice to use Reduced Web Beam Sections (RWBS) in steel moment resisting frames. Perforation of beam web in these members may cause stress and strain concentration around the opening area and facilitate ductile fracture under cyclic loading. This paper presents a numerical study on the cyclic fracture of these structural components. The considered connections are configured as T-shaped assemblies with beams of elongated circular perforations. The failure of specimens under Ultra Low Cycle Fatigue (ULCF) condition is simulated using Cyclic Void Growth Model (CVGM) which is a micromechanics based fracture model. In each model, CVGM fracture index is calculated based on the stress and strain time histories and then models with different opening configurations are compared based on the calculated fracture index. In addition to the global models, sub-models with refined mesh are used to evaluate fracture index around the beam to column weldment. Modeling techniques are validated using data from previous experiments. Results show that as the perforation size increases, opening corners experience greater fracture index. This is while as the opening size increases the maximum observed fracture index at the connection welds decreases. However, the initiation of fracture at connection welds occurs at lower drift angles compared to opening corners. Finally, a probabilistic framework is applied to CVGM in order to account for the uncertainties existing in the prediction of ductile fracture and results are discussed.

**Keywords:** ultra low cycle fatigue; cyclic void growth model; perforated beams; fracture; finite element analysis

### 1. Introduction

It is common practice to provide web openings in floor beams for different purposes (Liu and Chung 2003). Elastic theory indicates that including holes in the beam web might cause stress concentrations in the remaining web material (Prinz and Richards 2009). For over 100 years the influence of creating openings on the elastic and plastic stress distribution has been studied by different researchers (Verweij 2010). The most recent studies on this topic has been focused on stress and strain distribution around the opening (Tsavdaridis *et al.* 2014, Lawson *et al.* 2015), optimization of perforation shape (Tsavdaridis and D'Mell 2012a, Akrami and Erfani 2015a), stability of perforated section (Tsavdaridis and D'Mell 2011, Akrami and Erfani 2015a), development of behavioral models (Chung 2012, Tsavdaridis and D'Mell 2012b), and etc. Most of

---

\*Corresponding author, Assistant Professor, E-mail: [sderfani@aut.ac.ir](mailto:sderfani@aut.ac.ir)

<sup>a</sup> Ph.D. Candidate, E-mail: [v.akrami@aut.ac.ir](mailto:v.akrami@aut.ac.ir)

these studies have reported the potential vulnerability of perforated sections to stress and strain concentrations as well as to local instabilities around the opening which shows that the fracture behavior of these structural components under seismic loading deserves a deeper study.

Components of steel structures may experience large amplitude cyclic straining during an earthquake. Under these strain amplitudes which can be several times of the yield strain, the ductile fracture initiates within a few cycles. Generally, the fracture under earthquake loading can be categorized into Ultra Low Cycle Fatigue (ULCF) condition (Zhou *et al.* 2012). Traditional fracture mechanics, including linear elastic approaches like stress intensity factor  $K$  or elasto-plastic approaches such as the J-integral or the Crack Tip Opening Displacement (CTOD) can predict fracture in situations with limited yielding and the presence of an initial crack (Tehrani-zadeh *et al.* 2012). Some recent studies using these methods can be found in (Huang *et al.* 2004, Singh *et al.* 2011, Kumar *et al.* 2014). However these assumptions are of limited use for ductile fracture under ULCF (Zhou *et al.* 2012). In addition, ductile fracture under earthquake loading generally occurs within a limited number of cycles which make it difficult to use some techniques required by traditional models (e.g., rain-flow cycle counting method and strain-life approach).

There are a number of methods for modeling ductile fracture of steel components under ULCF condition. One of the most recent models is the Cyclic Void Growth Model (CVGM) which has been developed based on its earlier version called Void Growth Model (VGM). Kanvinde and Deierlein (2004) developed VGM for monotonic loadings, based on the previous researches of Rice and Tracey (1969) and Hancock and Mackenzie (1976). They extended their idea to cyclic loads by considering effects of reversing loads on the growth and coalescence of micro-voids and developed CVGM (Kanvinde and Deierlein 2004, 2007). CVGM is a micromechanical based fatigue model proposed to simulate ductile fracture initiation due to large amplitude cyclic straining in structural steels.

In this paper, ductile fracture of perforated steel beams under Ultra-Low Cycle Fatigue (ULCF) condition is simulated using Cyclic Void Growth Model (CVGM). For this purpose, three dimensional finite element models of T-shaped connections with perforated beams are established and analyzed under cyclic loading. In addition to the global models, sub-models with refined mesh are used to evaluate fracture index around the beam to column weldment. Modeling techniques are validated using data from previous experiments. The state of fracture index at opening corners and connection welds are calculated and discussed for specimens with different perforations. In addition, the moment transferred to connection welds is calculated and it is shown that when this moment is less than effective plastic moment capacity of the connection, the fracture index at connection welds is acceptable. At the end, a probabilistic framework is applied to CVGM in order to account for the uncertainties existing in the prediction of ductile fracture and results are discussed. The parameters, assumptions, modeling techniques and obtained results are presented in the following sections.

## 2. Theory of CVGM model

Currently, the tools used by structural engineers to predict model failure are not as sophisticated as other aspects of structural analysis. Common methods used for fracture prediction contain varying degrees of empiricism rather than fundamental mechanics (Fell 2008). Simple approaches for prediction of ductile damage involve using the equivalent plastic strain or

dissipated energy as an indicator of damage. While these methods may give a rough prediction of tolerated damage, they fail to incorporate the effects of local buckling and the complex interactions of stress and strain histories that trigger fracture in the model. In this study, the failure of specimens under ULCF condition is modeled using CVGM which is a micromechanics-based model for prediction of fracture in steel material. With this approach, stress and strain histories that trigger fracture during an earthquake loading can be modeled directly.

From the perspective of micromechanics, ductile fracture in steel material is caused by the processes of void nucleation, growth, and coalescence (Myers *et al.* 2009). Fig. 1 displays different stages of ductile fracture in a perforated steel beam. Previous researches (Rice and Tracey 1969) have shown that the process of ductile fracture is highly related to the plastic strain and stress triaxiality around the voids. Accordingly, Kanvinde and Deierlein (2004) have suggested that the cyclic void growth demand,  $VGD_{cyclic}$ , can be calculated using the following equation

$$VGD_{cyclic} = \sum_{tensile} \int_{\epsilon_1}^{\epsilon_2} \exp(|1.5T|) d\epsilon_p - \sum_{compressive} \int_{\epsilon_1}^{\epsilon_2} \exp(|1.5T|) d\epsilon_p \geq 0 \tag{1}$$

In this equation,  $T$ , is the stress triaxiality ( $T = \sigma_m/\sigma_e$ ),  $\sigma_m$ , is the mean stress,  $\sigma_e$ , is the effective Von-Mises stress and  $d\epsilon_p$  is the incremental equivalent plastic strain. Also, based on the findings of Rice and Tracey (1969) they have concluded that the void growth capacity,  $\eta_{cyclic}$ , decreases exponentially with plastic strain while the stress triaxiality is negative (Kanvinde and Deierlein 2004)

$$\eta_{cyclic} = \exp(-k\epsilon_c) \eta_{monotonic} \tag{2}$$

where,  $k$  stands for the material dependent damageability coefficient,  $\epsilon_c$  is the equivalent plastic strain determined at reversal points from a negative to positive triaxiality and  $\eta_{monotonic}$  is the void growth capacity in monotonic tensile loading. According to CVGM, ductile fracture under cyclic loading initiates when the fracture demand exceeds the fracture capacity over the characteristic length, or when the ratio between the fracture demand and existing fracture capacity exceeds unity over the characteristic length

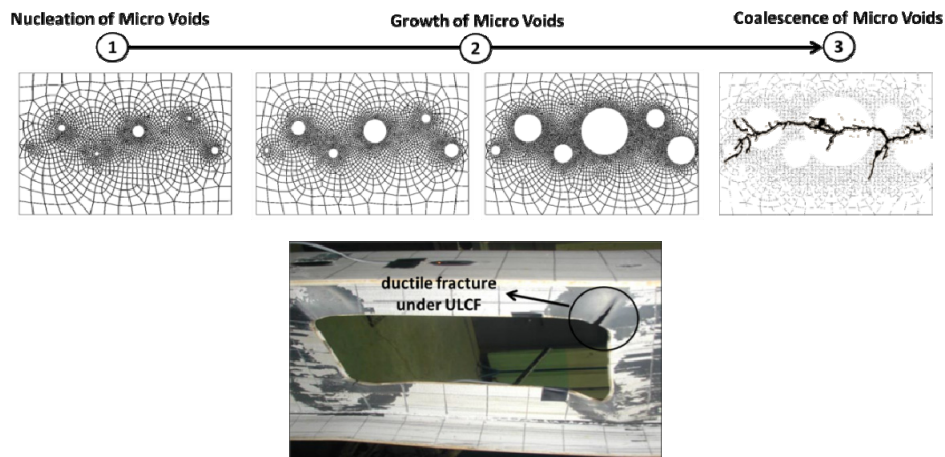


Fig. 1 Micromechanical process of ductile fracture (test conducted by Lee *et al.* (2004))

$$FI_{cyclic} = VGD_{cyclic} / \eta_{cyclic} \geq 1.0 \quad (3)$$

The characteristic length is a material dependent parameter which its choice of determination is based on the microstructural measurements as well as finite element (FE) analyses (see sub-section 3.3).

### 3. Modeling strategy

#### 3.1 Geometry and constraints

The considered connection assembly represents an exterior T-shaped connection isolated from a moment frame which has been tested under cyclic loading by Shinde *et al.* (2003). The assembly consists of the half beam span and half the column height on each side of the beam. This is because for a moment frame under lateral loading, the inflection points of the column and the beam rest at the mid-height of the column and the half-span of the beam. Fig. 2 displays geometry of the connection and the parameters used to model web openings. According to the previous studies, round openings perform better than rectangular openings of similar or smaller size (Akrami and Erfani 2015a). Therefore, in the present study, all openings have round corners producing vertical elongated circular ( $a < h$ ), circular ( $a = h$ ), and horizontal elongated circular ( $a > h$ ), shapes. The distance between the nearest point of the opening and the column edge is assumed to be equal to the depth of beam (i.e.,  $l = 0.5$  m). This is done as per AISC's design guide for steel and composite beams with web openings (Darwin 1990). Openings are concentric to the mid-height of the section with heights between  $0.4H$  and  $0.8H$  and lengths between  $0.5H$  and  $1.0H$ , where,  $H$ , is the depth of the sections. No opening reinforcement is considered. Effects of loading ram and supports are simulated using displacement constraints at the end of beam and columns. Load history recommended in ANSI/AISC341 (2010) is used for cyclic analyses (see Fig. 2(b)).

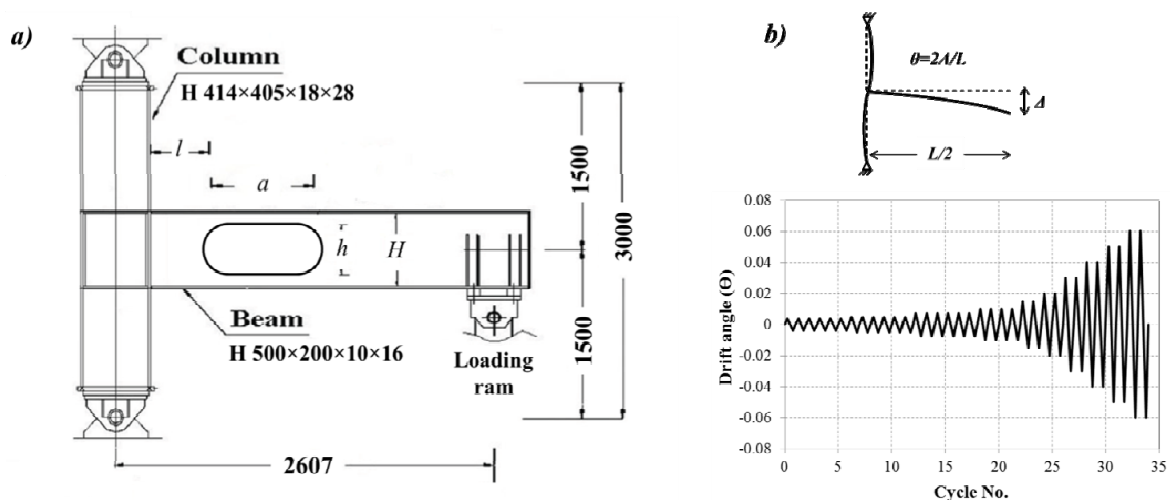


Fig. 2 Modeling of beam-to-column connection: (a) Details of models (Dimensions in mm); (b) cyclic loading protocol of ANSI/AISC341 (2010)

Table 1 Material properties of weld, base and HAZ regions (Liao and Wang 2010, Zhou *et al.* 2012)

Material	$E$ (GPa)	$\nu$	$\sigma_y$ (MPa)	$\sigma_u$ (MPa)	$\epsilon_u$	$\eta_{monotonic}$	$k$
Base metal	206	0.3	359.9	646.6	0.2	2.50	0.15
HAZ	206	0.3	375.7	631.2	0.2	2.40	0.20
Weld metal	206	0.3	391.4	615.8	0.2	2.52	0.15

### 3.2 Material properties

Both material and geometric nonlinearity are incorporated in the analysis. The material nonlinearity is based on a von Mises yield surface and an associated flow rule. Plastic hardening is modeled using combined isotropic-kinematic hardening law. The grade of steel for tested beams and the welding electrodes used for fabricating specimens have been reported as SN490B ( $F_y = 345$  Mpa) and YGW11 ( $F_y = 390$  MPa), respectively (Kurobane *et al.* 2004, Azuma *et al.* 2006). For verification of models, the mechanical properties of steel and weld metals are taken from the test results reported in (Kurobane *et al.* 2004). However, as the parameters of the cyclic fracture model are not reported for these materials, the mechanical properties and parameters of the cyclic fracture model for steel and weld metals are taken from the references (Liao and Wang 2010, Zhou *et al.* 2012) to be used in parametric studies. The mechanical properties for heat affected zone (HAZ) are taken as the average of those of base and weld metals. The parameters of the cyclic fracture model for HAZ are taken from (Liao and Wang 2010). Table 1 lists the material properties of weld, base and HAZ regions used in parametric studies.

According to some studies, yielding in the web at low rotations introduces sufficient asymmetry to trigger inelastic buckling at larger rotations, without having initial imperfections specified at the beginning (Prinz and Richards 2009). However, in this study the imperfect model is used in the analyses to take local and lateral buckling into account. In this method, first the buckling mode-shapes are computed in a separate buckling analysis and then the original perfect geometry of the model is perturbed using the first buckling mode shape with a 1/1000 scale factor (Hedayat and Celikag 2009).

### 3.3 Mesh generation

Four-noded shell elements are used to model perforated beams. Each element is separated into five layers across the thickness. Fig. 3(a) displays a typical mesh for numerical models. A detailed global and local mesh refinement studies are performed according to which, a global mesh of 20 mm  $\times$  20 mm is found suitable for parts with low or moderate strain gradients (Fig. 3(b)). Steep strain gradient at opening corners calls for greater nodal density around the holes. Fig. 3(c) displays results of mesh sensitivity analysis for opening corners. Considering the computational expense of cyclic loading, the mesh size for opening corners is limited to the characteristic length required by CVGM which has been reported to be 0.1-0.3 mm for structural steel (Kanvinde and Deierlein 2004). In this study, the size of finest element at the edge of opening corners is limited to 0.2 mm. The mesh makes a transition to a coarser mesh until it reaches the global mesh size. The same mesh size is adopted for the weld access hole and the edge of the beam flange at the connection area.

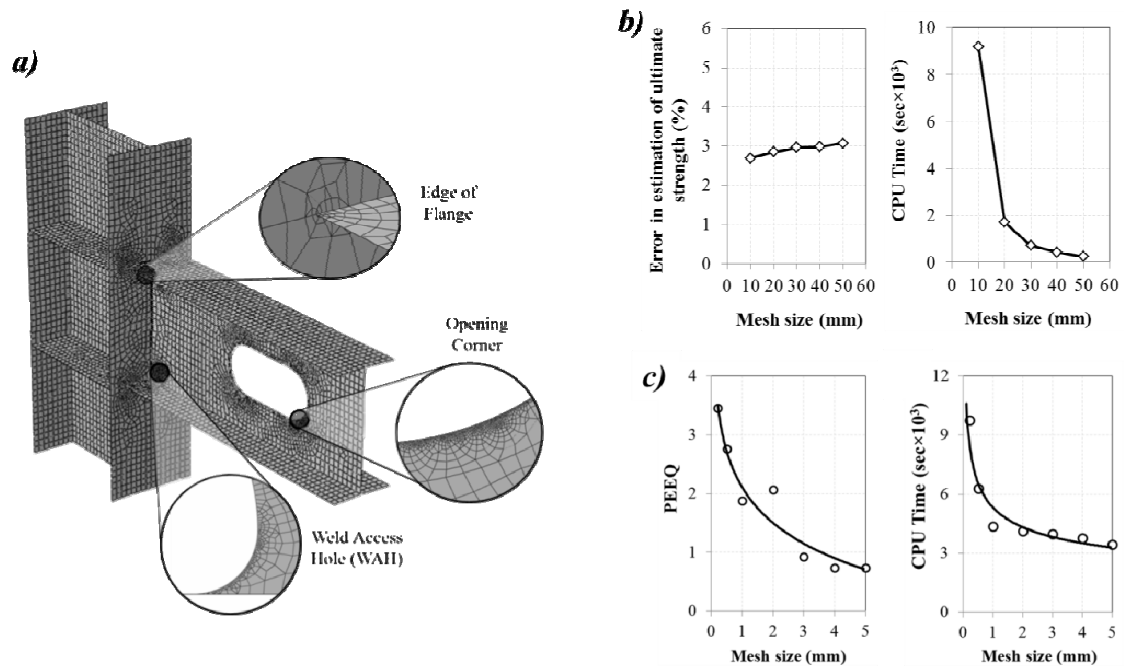


Fig. 3 Numerical modeling: (a) typical mesh of finite element models; (b) global mesh sensitivity analysis; (c) mesh sensitivity study for opening corners

### 3.4 Sub-models of beam-to-column connection zone

In addition to global shell model, a refined sub-model with solid elements is provided for simulation of beam-to-column connection zone. Displacement fields calculated by the shell model are used to drive the boundary nodes of the sub-model. Generally, three different sub-models are considered. Fig. 4 illustrates dimensions of weldments in each sub-model along with the corresponding FE model. The first two sub-models represent connections with partial joint penetration (PJP) groove welds which have been tested by Shinde *et al.* (2003) to study applicability of PJP groove welds to beam-column connections under seismic loads. These sub-models are used to verify the numerical modeling techniques used in this study. The third sub-model represents a beam-to-column connection with a complete joint penetration (CJP) groove weld. Since, for most of the beam-to column connections CJP groove welding is being used, this type of welding is considered for studying perforated specimens. For PJP and CJP groove welds the mechanical properties of weld material are used as reported in (Kurobane *et al.* 2004) and Table 1, respectively. For both models the parameters of the cyclic fracture model are used according to Table 1. As earlier studies show that fracture initiation is not likely to occur at the boundary between HAZ and base metal (Myers *et al.* 2009), this boundary is not modeled in simulations. Hence, the HAZ material is used for the beam and column flanges in sub-models.

### 3.5 Verification of the reference model

To check the modeling techniques used in this study, the reference model is subjected to cyclic loading and results are compared to the full-scale test data reported by Shinde *et al.* (2003).

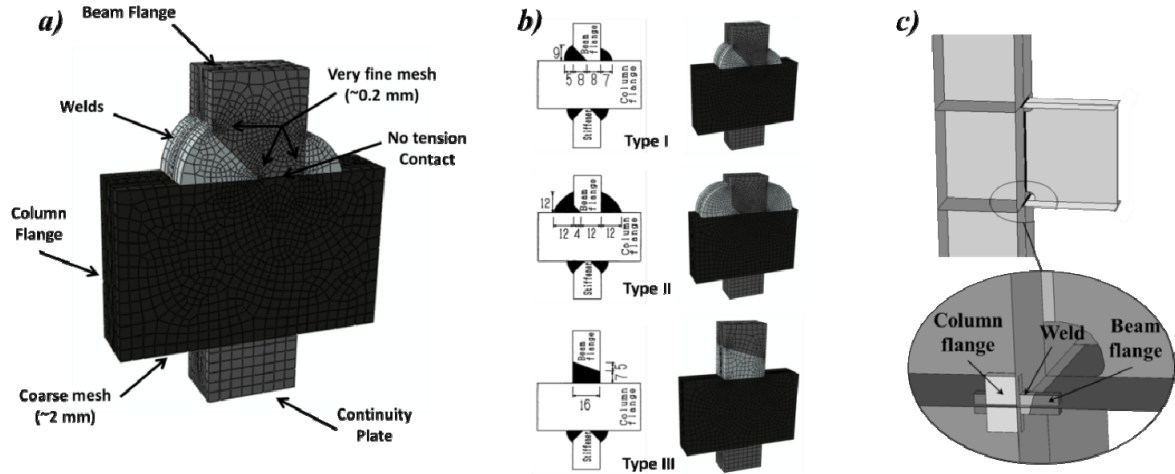


Fig. 4 Modeling of beam to column connection zone: (a) details of sub-models (mm); (b) weldment types; (c) positioning of sub-models with respect to the global model

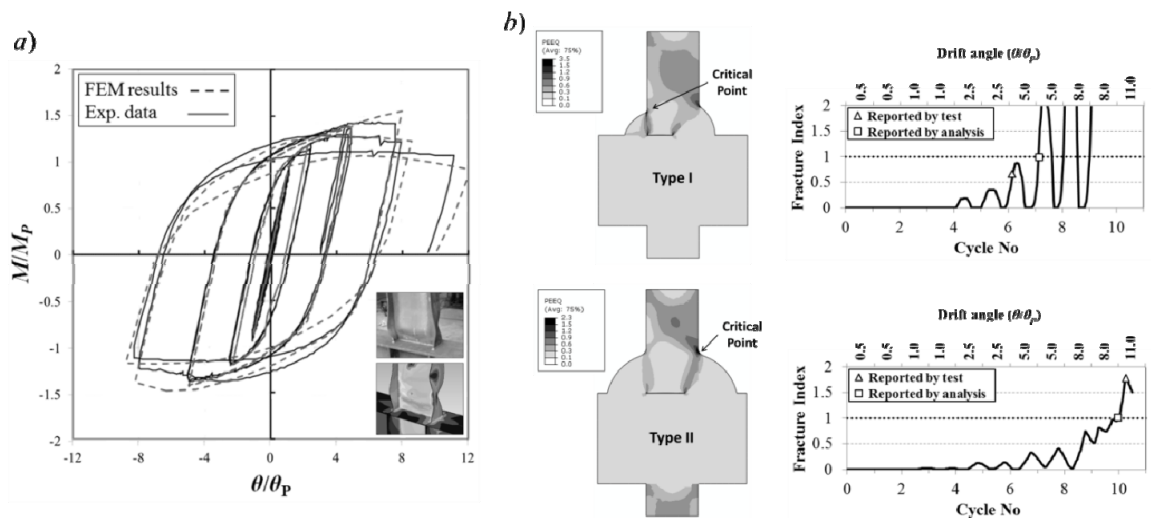


Fig. 5 Comparison of results from FEM and laboratory test: (a) global behaviour; (b) sub-model of beam-to-column connection zone

Hysteresis loops obtained from FE analysis and laboratory test are plotted in Fig. 5(a). As shown in this figure, the predicted load-displacement curve and buckling shape of the connection coincide well with the test results. Also, to validate results predicted by CVGM, the sub-models type I and II are analyzed and calculated fracture time is compared to the existing experimental data (Shinde *et al.* 2003). Fig. 7(b) displays growth of CVGM fracture index at the most critical point for both models. As shown in the figure, for sub-model II the fracture time predicted by CVGM is close to that observed in the lab test. However, for sub-model I, CVGM predicts the initiation of fracture one cycle after the actual fracture time observed in the experiments. After-test studies conducted by Shinde *et al.* (2003) have shown that the premature failure of this specimen was due to

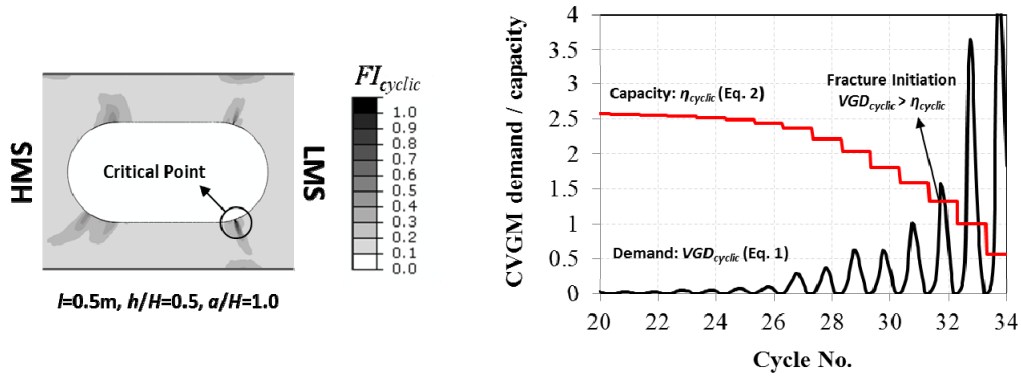


Fig. 6 Damage evolution for the most critical element around the opening

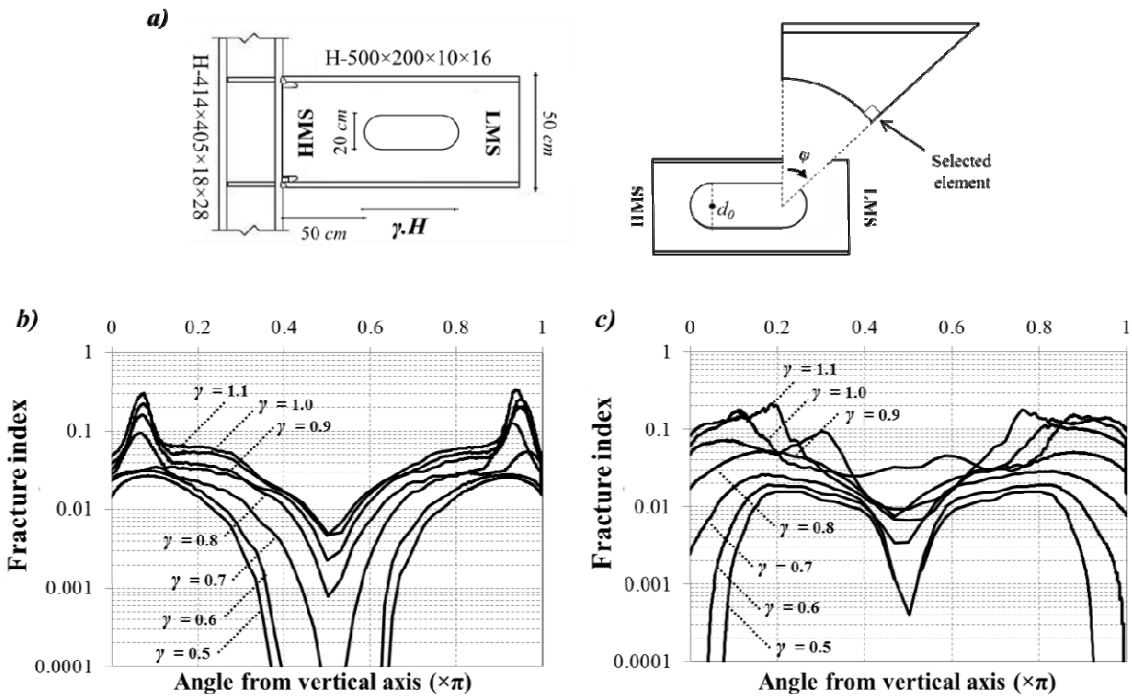


Fig. 7 Fracture index around the opening (drift 0.04 rad): (a) opening configuration; (b) fracture index at LMS; (c) fracture index at HMS

incomplete penetration of the weld metal at connection area.

#### 4. Results

##### 4.1 State of fracture index around the opening

The stress and strain time histories of the elements in the FE model are monitored to calculate the CVGM damage index for each element of the model at each time step. This is done using a

computer code developed by authors. Fig. 6 displays an example of damage evolution for the most critical element around the opening. The fracture demand,  $VGD_{cyclic}$ , increases and decreases during the tensile and compressive loadings, respectively (Eq. (1)). On the other hand, the void growth capacity,  $\eta_{cyclic}$ , decreases exponentially with plastic strain while the stress triaxiality is negative (Eq. (2)). Referring to the figure, ductile fracture initiates when the fracture demand exceeds the fracture capacity. To predict the initiation of ductile fracture, a more common index named as adjusted fracture index (simply called fracture index) has been introduced which refers to the ratio between the fracture demand and existing fracture capacity (Eq. (3)). CVGM states that failure under ULCF occurs once the CVGM fracture index exceeds unity over the characteristic length.

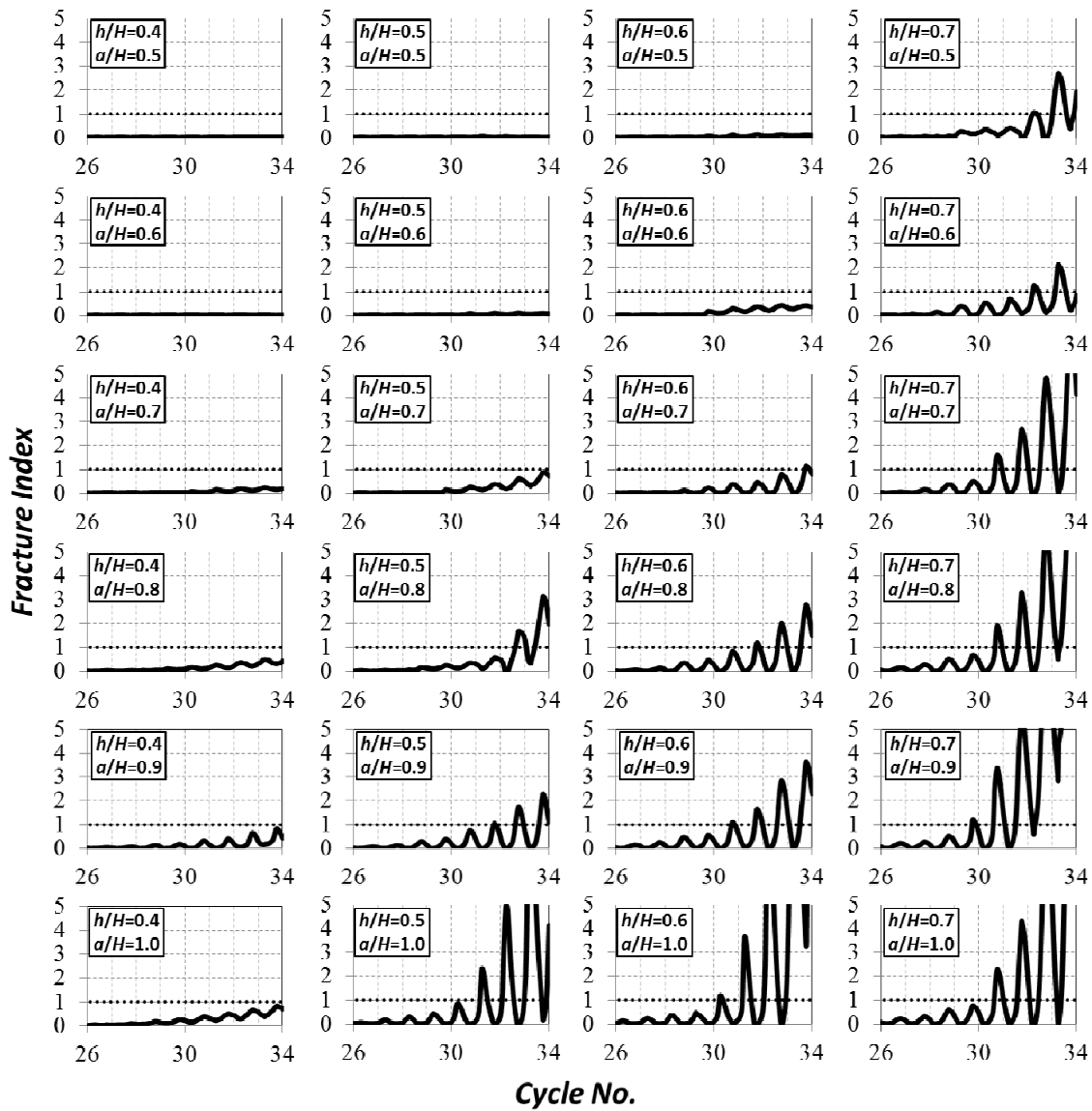


Fig. 8 Time history of fracture index at the most critical element around the opening of each model

Fig. 7 displays the state of fracture index ( $FI_{cyclic}$ ) at the circular parts of the perforation where the most critical element is supposed to be within (drift 0.04 rad). Fig. 7(a) shows the configuration of considered openings. As it is clear from the figure, all perforations have the same height of 200 mm ( $h/H = 0.4$ ) while their length is being changed. Fig. 7(b) illustrates the state of fracture index at low moment side (LMS) of the opening, from which it can be seen that the location of most critical element at LMS is almost constant. However, the value of fracture index at the most critical element increases as the opening length increases. Fig. 7(c) displays the same graph for high moment side (HMS) of the opening. According to the figure, the critical fracture index at HMS spreads over a wider range of elements. Also, it is evident that as the opening length increases, the maximum fracture index keeps growing and moving towards the start and end of the circular part while its value becomes more uniform. However, for long openings distribution of fracture index becomes irregular which is mainly due to the occurrence of local web buckling at the HMS.

Time history of the CVGM fracture index at the most critical element around the opening is plotted for each model and presented in Fig. 8. As shown in the figure, for models with small perforation, generally there is no sign of ductile fracture around the opening. However, as the length or height of opening increases the maximum experienced fracture index around the opening becomes larger. Based on the graphs, all specimens with  $h/H = 0.7$  experience ductile fracture around their openings. However, as the opening length of these models increases, the ductile fracture initiates at lower loading level (drift angle). For models with  $h/H = 0.5$  and  $h/H = 0.6$ , the initiation of ductile fracture around the opening depends on the opening length. For both sets of models as the opening length exceeds  $a/H \geq 0.7$  the opening zone experiences ductile fracture. For models with opening height less than  $0.4H$  ductile fracture does not occur around the opening ( $0.5 \leq a/H \leq 1.0$ ).

#### 4.2 State of fracture index at connection welds

For each specimen, the sub-model with CJP groove weld (type III) is placed at the critical flange corner determined by the analysis of global model to calculate fracture demand,  $VGD_{cyclic}$ , and void growth capacity,  $\eta_{cyclic}$ . Fig. 9 shows fracture demand and void growth capacity for original connection without web opening. For this model the initiation of ductile fracture occurs during the first cycle to 3% drift angle. As shown in the figure, there is a significant strain concentration at the toe of weld where ductile fracture initiates. From the theoretical point of view

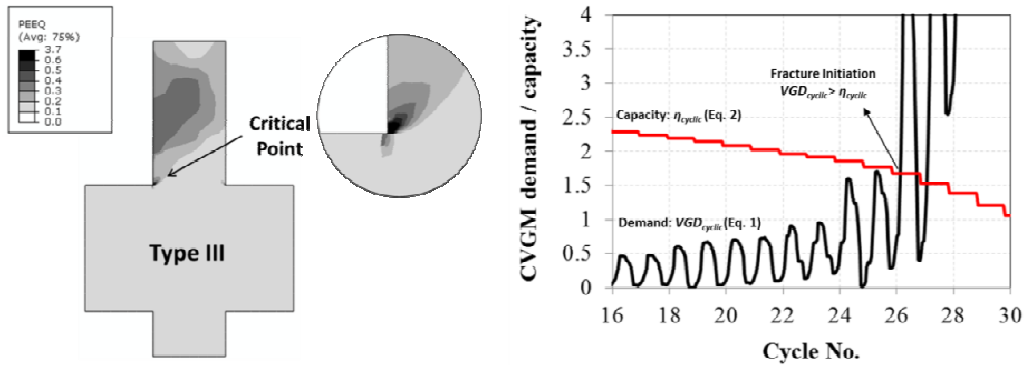


Fig. 9 Damage evolution for the most critical element at connection welds

models with smoother weld toe may result in lower strain concentrations at this area; however, as in the real process the cross section of the connecting part between the beam flange and the column flange may differ significantly from case to case, the idealized geometry of the CJP weld is used in this study.

Time history of the fracture index at the most critical element is plotted for different models and presented in Fig. 10. According to the figure, openings with small dimensions have no considerable effect on the state of fracture index at connection welds. Same as for un-perforated beam, the initiation of ductile fracture for these specimens occurs during the first cycle to 3% drift angle. As discussed in the previous sub-section, for these models opening corners do not

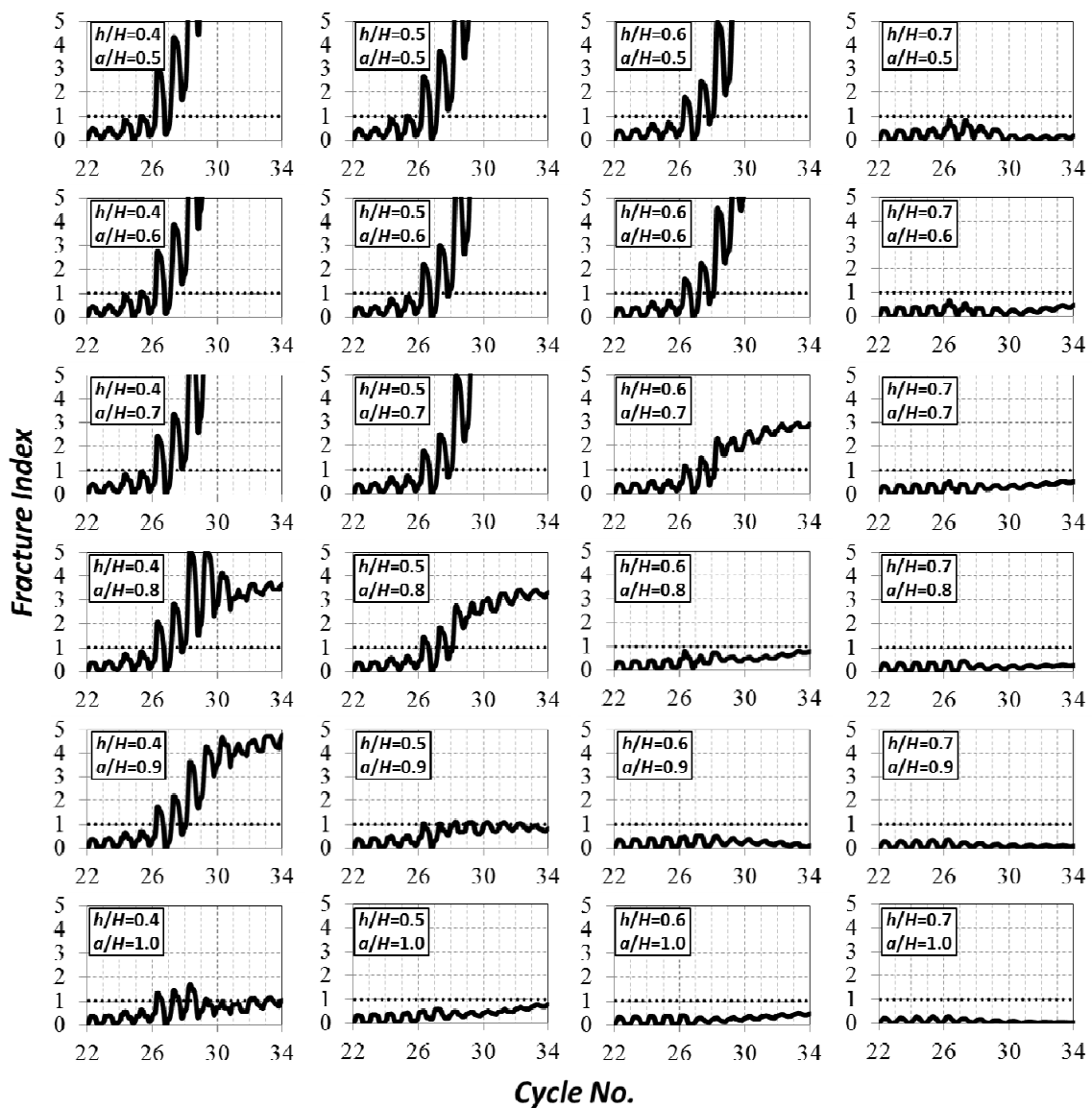


Fig. 10 Time history of fracture index at the most critical element connections welds

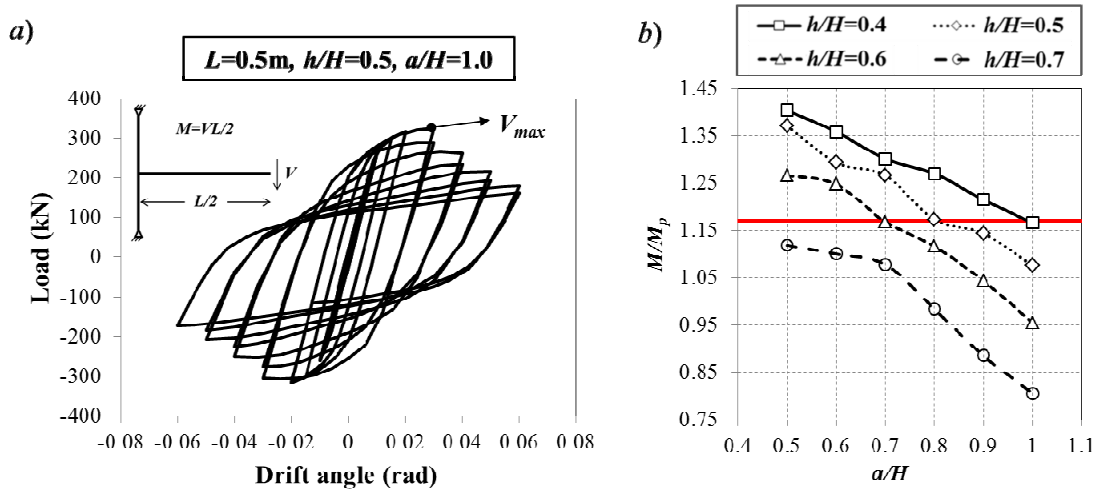


Fig. 11 Maximum moment transferred to connection welds for studied models

experience ductile fracture. However, as the opening size increases the fracture index at connection welds decreases gradually. This can be due to formation of Vierendeel mechanism at opening area which shifts the location of maximum deformation demand from the welded section to the perforated zone. For specimens with  $h/H = 0.7$  no ductile fracture occurs at connection welds. However, for openings with  $h/H = 0.6$  and  $h/H = 0.5$  the connection welds become safe when  $a/H \geq 0.8$  and  $a/H \geq 1.0$ , respectively. For specimens with opening height equal to  $0.4H$ , as the perforation length increases the fracture index at connection welds decreases, but for all studied openings it is still more than unity.

By comparing state of fracture at opening corners and connection welds (i.e., Figs. 8 and 10) it can be said that the initiation of fracture at connection welds occurs at lower drift angles. From the design point of view, it is desirable to have connection welds with least susceptibility to ULCF. In order to find a rule for reduction of fracture index at connection welds, maximum moment transferred to connection welds,  $M$ , are calculated for different models and plotted in Fig. 11. Calculated values are normalized using plastic moment capacity of the connection,  $M_p$ , which is defined as the plastic section modulus times the measured material yield strength. The reference line plotted in this figure corresponds to the effective plastic moment capacity of the connection,  $M_{p,e}$ , which is larger by a small amount than the calculated plastic moment capacity  $M_p$  due to cyclic hardening of steel material. Lignos and Krawinkler (Lignos and Krawinkler 2011) have shown that the mean ratio between effective and calculated plastic moment capacity,  $M_{p,e}/M_p$ , is about 1.17. Comparing Figs. 10 and 11, it can be said that when transferred moment to connection welds is less than effective plastic moment capacity of the connection, the fracture index at connection welds is in an acceptable level.

#### 4.3 Probabilistic framework

Generally, there are several sources of uncertainty in the ductile fracture prediction process. The main sources of uncertainty arise from variations in geometry of the specimen, random nature of earthquake loading, idealization of specimen during FE modeling, material variability, extraction of fracture parameters and uncertainty in the fracture process itself. In order to account

for uncertainties existing in the prediction of ductile fracture, it is helpful to apply a probabilistic framework to CVGM. However, it is not practical to investigate all sources of uncertainties in this study; instead an attempt is made to evaluate effect of uncertainties existing in calculation of fracture demand,  $VGD_{cyclic}$ , and capacity,  $\eta_{cyclic}$ , which may be accountable for material variability, uncertainty in extraction of fracture parameters and uncertainty in the fracture process itself. For this purpose, Eq. (3) is rewritten in the form

$$FI_{cyclic} = \frac{\beta \sum_{tensile} \int_{\epsilon_1}^{\epsilon_2} \exp(|A \cdot T|) d\epsilon_p - \sum_{compressive} \int_{\epsilon_1}^{\epsilon_2} \exp(|A \cdot T|) d\epsilon_p}{\exp(-k\epsilon_c) \cdot \eta_{monotonic}} \quad (4)$$

In which four deterministic parameters of the CVGM, namely  $A$ ,  $\beta$ ,  $k$  and  $\eta_{monotonic}$ , are considered as random variables. The parameter,  $A$ , controls the influence of stress triaxiality on growth and reduction of fracture demand. Rice and Tracey (1969) have proposed a value of 1.5 for this parameter. However, later studies have shown that this parameter can be as less as 1.3 for specimens with low stress triaxiality (Smith *et al.* 2014). In this study, three different values, 1.3, 1.4 and 1.5 are considered for this random variable. The parameter,  $\beta$ , governs the relative rate of damage accumulation and reduction. In the original model, this parameter is set to 1.0; However it is suggested that this parameter may have a higher values, which are lognormal distributed around 1.0 (Smith *et al.* 2014). This parameter is also assumed to take three different values, 1.0, 1.05 and 1.1. In order to account for uncertainties inherent in fracture parameters,  $k$  and  $\eta_{monotonic}$ , these random variables are assumed to take different values as obtained by Liao and Wang (2010) during lab tests. For each element inside the model, fracture index can be calculated using different combinations of introduced random variables. Fig. 12 illustrates time histories of fracture index plotted for different combinations of random variables. Graphs are presented for both opening corner and connection welds considering models with  $a/H = 1.0$  and three different height factors. As can be seen in the figure, at each loading level some curves are above the fracture line ( $FI_{cyclic} =$

Table 2 Different values of fracture parameters for materials listed in Table 1 (Liao and Wang 2010)

No.	Base metal		HAZ		Weld metal	
	$k$	$\eta_{mon}$	$k$	$\eta_{mon}$	$k$	$\eta_{mon}$
1	0.560	2.29	0.567	2.47	0.297	2.69
2	0.638	2.53	0.747	2.41	0.189	2.43
3	0.144	2.41	0.365	2.30	0.495	2.44
4	0.193	2.48	0.303	2.36	0.315	2.28
5	0.058	2.62	0.443	2.56	0.064	2.80
6	0.067	2.69	0.144	2.32	0.074	2.48
7	0.221	-	0.178	-	0.155	-
8	0.245	-	0.607	-	0.128	-
9	0.361	-	0.329	-	0.426	-
10	0.108	-	0.227	-	0.165	-
11	0.137	-	0.317	-	-	-
12	-	-	0.154	-	-	-

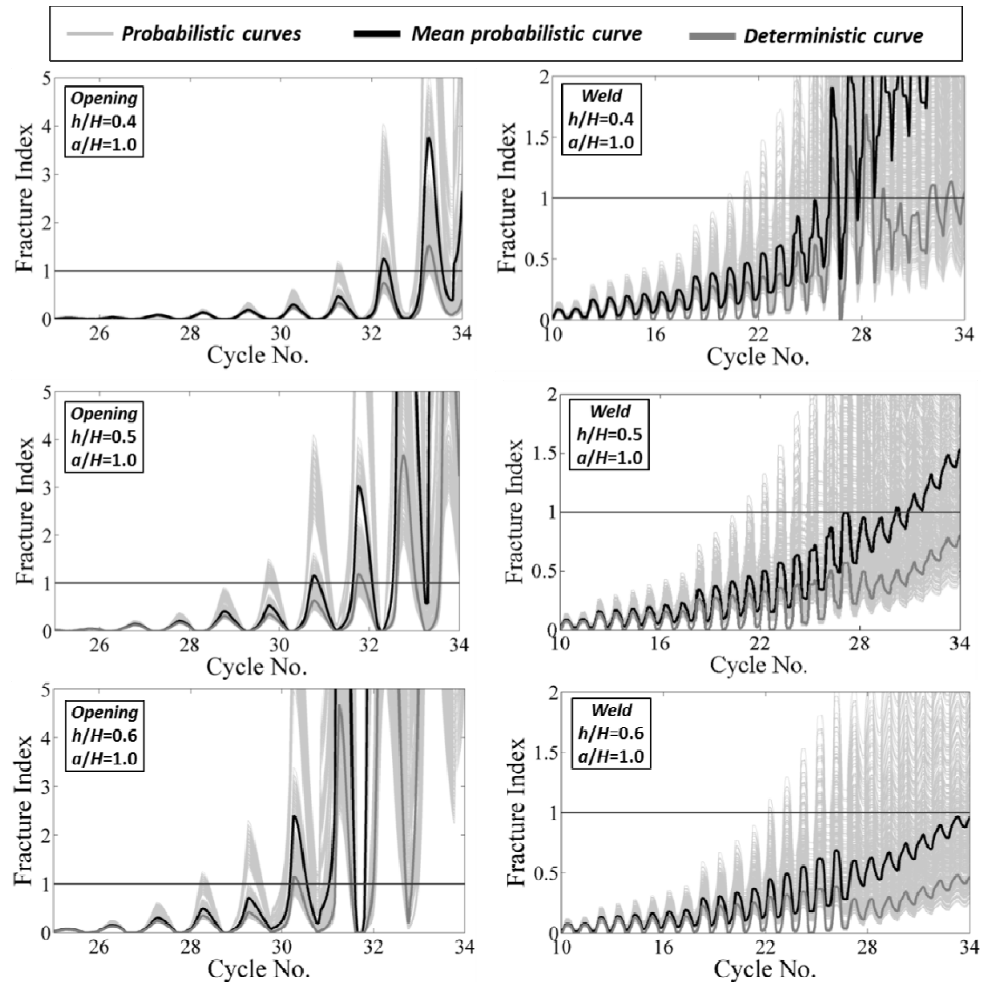


Fig. 12 Fracture index plotted for different combinations of random variables ( $a/H = 1.0$ )

1.0) while for some other combinations of random variables the resultant curve remains under critical value.

At each step of analysis, the probability of failure may be calculated as the ratio between number of simulations leading to failure and the total number of iterations

$$P_f = \frac{N(FI_{cyclic} > 1.0)}{N_{Total}} \quad (5)$$

where,  $N(FI_{cyclic} > 1.0)$ , is the number of curves that has passed the line  $FI_{cyclic} = 1.0$ , at least one time and,  $N_{Total}$ , is the total number of curves. Fig. 13 displays growth of failure probability for specimens with  $a/H = 1.0$ , during the cyclic loading. According to the figure, as the opening height increases the probability of failure at opening corners increases. However, the probability of failure is equal to zero before cycle #28 (the first cycle to 4% drift angle). This is while as the opening height increases the probability of failure decreases at connection welds. It is worth noting

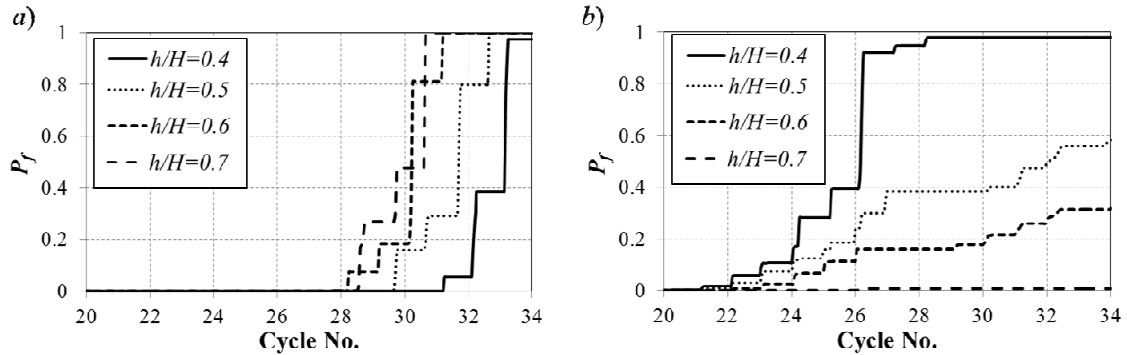


Fig. 13 Time history of failure probability for models with  $a/H = 1.0$ : (a) opening corners; (b) connection welds

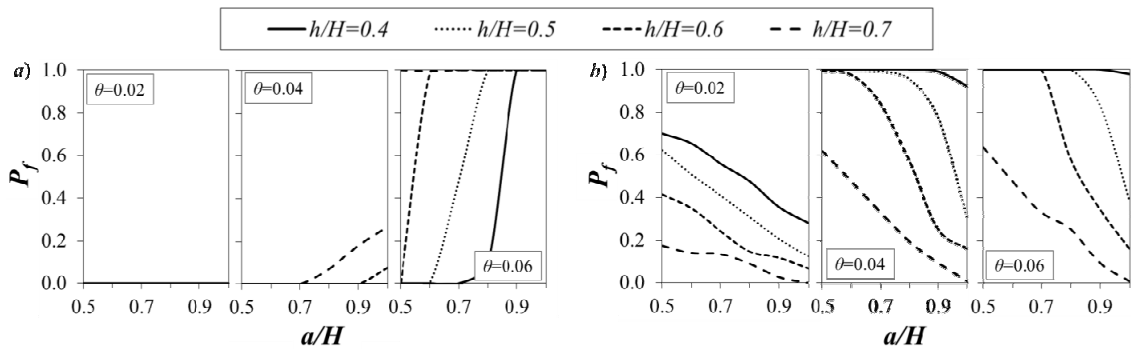


Fig. 14 Probability of failure at different loading levels: (a) opening corners; (b) connection welds

that the probability of failure at connection welds starts to increase at lower levels of drift angle compared to the opening corners. The maximum probability of failure at opening corners and connection welds is obtained for studied models during the last cycle at three different drift angles and plotted in Fig. 14. Again, it can be seen that the probability of failure at connection welds starts to increase at lower drift angles compared to the opening corners. Considering the last graph in Fig. 14(a), for a given opening height, it is unlikely to have ductile fracture at opening corners while the opening length is less than a specific value. Beyond this value, probability of failure increases until it reaches the unity meaning that for corresponding models the opening corners will definitely experience ductile fracture. Fig. 14(b) shows the same results for connection welds from which it can be deduced that as the opening size increases the probability of ductile fracture at connection welds decreases. However, even for the largest perforation studied in this paper, there is still a small probability that the failure will occur at connection welds.

### 5. Discussion

Results presented in previous sections showed that introducing a web opening with certain dimensions can actually result in avoiding brittle connection weld fracture. Generally, this can be due to formation of Vierendeel mechanism at opening area which shifts the location of maximum

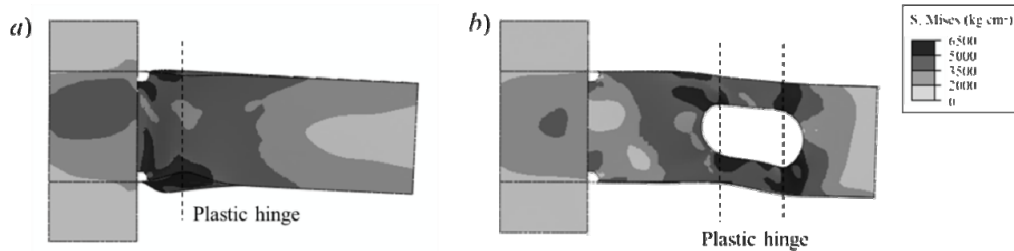


Fig. 15 Location of the plastic zone for: (a) original connection without web opening; (b) perforated model with  $a/H = 0.9$  and  $h/H = 0.5$

deformation demand from the welded section to the perforated zone. Fig. 15 demonstrates the location of the plastic zone at 0.04 rad drift angle for original connection without web opening and a perforated model with safe connection zone ( $a/H = 0.9$ ,  $h/H = 0.5$ ). Fig. 15(a) shows formation of plastic hinge at the end of original non-perforated beam. According to ANSI/AISC358 (2010), for welded moment connections the portion of beam extending one beam depth,  $H$ , from the face of the column should be treated as a protected zone. Since during a major earthquake, a plastic hinge is expected to form in this area, the use of perforated sections is not permitted in this zone (ANSI/AISC341 2010). As it can be seen in Fig. 15(a), this area experiences significant yielding and large inelastic deformations. However, for perforated model the inelastic deformations shift inside the beam and there is no plastic hinge at the end of the beam anymore (Fig. 15(a)). Comparing two aforementioned connections it can be said that, if it is intended to have a moment frame with traditional failure mechanism known by formation of two plastic hinges at both sides of the beams, then existence of large web openings even beyond the protected zone may be problematic. On the other hand a moment frame may be designed as a new lateral load resisting system based on the formation of Vierendeel mechanism at perforated sections and there will be no need to consider a protected zone at the ends of beams because there will be no plastic hinge at this zone.

To design such a lateral load resisting system, the size of web openings should be proportioned to limit the moment transferred to connection welds. For beams of a moment resisting frame designed to withstand both lateral and gravity loads, the maximum probable moment at the face of the column will be equal to

$$M = \frac{VL}{2} + \frac{qL^2}{12} \quad (6)$$

Where  $V$  is the shear load caused by seismic loads,  $L$  is the length of beam and  $q$  is the distributed linear gravity load on the beam. As mentioned before, the connection welds will be safe if the maximum moment at the face of the column does not exceed the effective plastic moment capacity of the beam ( $M < M_{p,e}$ ). An exclusive summary of existing methods which can be used to set fusing threshold of a perforated section to a predetermined value is presented in (Akrami and Erfani 2015b).

## 6. Conclusions

This paper aims at numerically investigating cyclic fracture of perforated steel beams. For this

purpose, three dimensional finite element models of T-shaped connections with perforated beams are established and analysed under cyclic loading. The failure of specimens under Ultra-Low Cycle Fatigue (ULCF) condition is modeled using Cyclic Void Growth Model (CVGM). In addition to the global models, sub-models with refined mesh are used to evaluate fracture index around the beam to column weldment. Based on the results, for models with small perforation ( $h/H \leq 0.6$ ,  $a/H \leq 0.7$ ), generally there is no sign of ductile fracture around the opening. However, as the opening length or height increases the maximum experienced fracture index around the opening exceeds the unity. On the other hand, as the opening size increases the fracture index at connection welds decreases gradually. This is due to formation of Vierendeel mechanism at opening area which shifts the location of maximum deformation demand from the welded section to the perforated zone. It is found that when the moment transferred to connection welds is less than effective plastic moment capacity of the connection, the fracture index at connection welds is in an acceptable level. At the end, a probabilistic framework is applied to CVGM and probability of failure is calculated for both opening corners and connection welds. Results show that based on the size of perforation, either the opening corners or connection welds will experience ductile fracture. However, the probability of failure at connection welds starts to increase at lower levels of drift angle compared to the opening corners.

## References

- Akrami, V. and Erfani, S. (2015a), "Effect of local web buckling on the cyclic behavior of reduced web beam sections (RWBS)", *Steel Compos. Struct., Int. J.*, **18**(3), 641-657.
- Akrami, V. and Erfani, S. (2015b), "Review and assessment of design methodologies for perforated steel beams", *J. Struct. Eng.*, 04015148. DOI: 10.1061/(ASCE)ST.1943-541X.0001421
- ANSI/AISC341 (2010), Seismic provisions for structural steel building; American Institute of Steel Construction (AISC), Chicago, IL, USA.
- ANSI/AISC358 (2010), Prequalified connections for special and intermediate steel moment frames for seismic applications; American Institute of Steel Construction (AISC), Chicago, IL, USA.
- Azuma, K., Kurobane, Y., Iwashita, T. and Dale, K. (2006), "Full-scale testing of beam-to-RHS column connections with partial joint penetration groove welded joints and assessment of safety from brittle fracture", *Weld. World*, **50**(5-6), 59-67.
- Chung, K. (2012), "Recent advances in design of steel and composite beams with web openings", *Adv. Struct. Eng.*, **15**(9), 1521-1536.
- Darwin, D. (1990), *Steel and Composite Beams with Web Openings*, Steel Design Guide Series 2, American Institute of Steel Construction (AISC), Chicago, IL, USA.
- Fell, B.V. (2008), "Large-scale testing and simulation of earthquake induced ultra low cycle fatigue in bracing members subjected to cyclic inelastic buckling", Ph.D. Dissertation; Civil and Environmental Engineering department, University of California, Davis, CA, USA.
- Hancock, J.W. and Mackenzie, A.C. (1976), "On the mechanisms of ductile failure in high-strength steels subjected to multi-axial stress-states", *J. Mech. Phy. Solids*, **24**(2-3), 147-160.
- Hedayat, A.A. and Celikag, M. (2009), "Post-northridge connection with modified beam end configuration to enhance strength and ductility", *J. Construct. Steel Res.*, **65**(7), 1413-1430.
- Huang, J., Nemat-Nasser, S. and Zarka, J. (2004), "Prediction of fatigue life of metallic structures with welded joints using automatic learning systems", *Int. J. Mech. Mater. Des.*, **1**(3), 255-270.
- Kanvinde, A.M. and Deierlein, G.G. (2004), "Micromechanical simulation of earthquake-induced fracture in steel structures", (John A. Blume), Earthquake Engineering Center Technical Report 145; Stanford Digital Repository.
- Kanvinde, A.M. and Deierlein, G.G. (2007), "Cyclic void growth model to assess ductile fracture initiation

- in structural steels due to ultra low cycle fatigue”, *J. Eng. Mech.*, **133**(6), 701-712.
- Kumar, S., Singh, I.V. and Mishra, B.K. (2014), “XFEM simulation of stable crack growth using J-R curve under finite strain plasticity”, *Int. J. Mech. Mater. Des.*, **10**(2), 165-177.
- Kurobane, Y., Azuma, K. and Makino, Y. (2004), “Applicability of PJP groove welding to beam-column connections under seismic loads”, *Connections in Steel Structures V*, Amsterdam, The Netherlands, June.
- Lawson, R.M., Basta, A. and Uzzaman, A. (2015), “Design of stainless steel sections with circular openings in shear”, *J. Construct. Steel Res.*, **112**, 228-241.
- Lee, E.T., Chang, K.H., Shim, H.J. and Kim, J.H. (2004), “Local buckling behavior of steel members with web opening under cyclic loading”, *Proceedings of the 7th Pacific Structural Steel Conference*, Chicago, IL, USA, March. Sponsored by: American Society of Civil Engineers (AISC)
- Liao, F.F. and Wang, W. (2010), “Parameter calibrations of micromechanics-based fracture models of Q345 steel”, *Sciencepaper*. URL: <http://www.paper.edu.cn/index.php/default/releasepaper/content/201007-457> [In Chinese]
- Lignos, D. and Krawinkler, H. (2011), “Deterioration modeling of steel components in support of collapse prediction of steel moment frames under earthquake loading”, *J. Struct. Eng.*, **137**(11), 1291-1302.
- Liu, T.C.H. and Chung, K.F. (2003), “Steel beams with large web openings of various shapes and sizes: Finite element investigation”, *J. Construct. Steel Res.*, **59**(9), 1159-1176.
- Myers, A.T., Deierlein, G.G. and Kanvinde, A.M. (2009), “Testing and probabilistic simulation of ductile fracture initiation in structural steel components and weldments”, (John A. Blume), Earthquake Engineering Center Technical Report 170; Stanford Digital Repository.
- Prinz, G.S. and Richards, P.W. (2009), “Eccentrically braced frame links with reduced web sections”, *J. Construct. Steel Res. (JCSR)*, **65**(10-11), 1971-1978.
- Rice, J.R. and Tracey, D.M. (1969), “On the ductile enlargement of voids in triaxial stress fields”, *J. Mech. Phys. Solids*, **17**(3), 201-217.
- Shinde, H., Kurobane, Y., Azuma, K. and Dale, K. (2003), “Additional full-scale testing of beam-to-column connections with improvements in welded joints”, *Proceedings of the 13th International Offshore and Polar Engineering Conference*, Honolulu, HI, USA, May.
- Singh, I.V., Mishra, B.K. and Bhattacharya, S. (2011), “XFEM simulation of cracks, holes and inclusions in functionally graded materials”, *Int. J. Mech. Mater. Des.*, **7**(3), 199-218.
- Smith, C.M., Deierlein, G.G. and Kanvinde, A.M. (2014), “A stress-weighted damage model for ductile fracture initiation in structural steel under cyclic loading and generalized stress states”, (John A. Blume), Earthquake Engineering Technical Report 187; Stanford Digital Repository.
- Tehranizadeh, M., Deylami, A., Gholami, M. and Moaze, H. (2012), “Validation of cyclic void growth model for fracture initiation in the flange plate connection between beam and box column”, *Proceedings of the 15th World Conference on Earthquake Engineering (15 WCEE)*, Lisbon, Portugal, September.
- Tsavdaridis, K.D. and D’Mello, C. (2011), “Web buckling study of the behaviour and strength of perforated steel beams with different novel web opening shapes”, *J. Construct. Steel Res.*, **67**(10), 1605-1620.
- Tsavdaridis, K.D. and D’Mello, C. (2012a), “Optimisation of novel elliptically-based web opening shapes of perforated steel beams”, *J. Construct. Steel Res.*, **76**, 39-53.
- Tsavdaridis, K.D. and D’Mello, C. (2012b), “Vierendeel bending study of perforated steel beams with various novel web opening shapes through nonlinear finite-element analyses”, *J. Struct. Eng.*, **138**(10), 1214-1230.
- Tsavdaridis, K.D., Faghih, F. and Nikitas, N. (2014), “Assessment of Perforated Steel Beam-to-Column Connections Subjected to Cyclic Loading”, *J. Earthq. Eng.*, **18**(8), 1302-1325.
- Verweij, J.G. (2010), “Cellular beam-columns in portal frame structures”, Master thesis, Civil Engineering Department, Delft University of Technology, The Netherlands.
- Zhou, H., Wang, Y., Shi, Y., Xiong, J. and Yang, L. (2012), “Extremely low cycle fatigue prediction of steel beam-to-column connection by using a micro-mechanics based fracture model”, *Int. J. Fatigue*, **48**, 90-100.